

Spectral Redshift in Harmonic Generation from Plasma Dynamics in the Laser Focus

F. Brandi,^{1,*} F. Giammanco,¹ and W. Ubachs²

¹Physics Department, University of Pisa, Largo B. Pontecorvo 3, 56127-Pisa, Italy

²Laser Centre, Vrije Universiteit Amsterdam, De Boelelaan 1081, 1081 HV Amsterdam, The Netherlands[†]

(Received 28 June 2005; published 30 March 2006)

High-precision spectral measurements on the 9th harmonic generated in xenon gas are compared with calculations of the plasma dynamics resulting from multiphoton ionization in the laser focus. For the regime of 300 ps pulses and above-saturation intensities a novel mechanism producing redshifts in the harmonics is uncovered and explained. Ions play a double role: the nonlinear susceptibility of the ions is decisive for the harmonic intensity, while their mutual repulsion and the associated increase of the index of refraction is identified as the cause of the redshift.

DOI: 10.1103/PhysRevLett.96.123904

PACS numbers: 42.65.Ky, 32.70.Jz, 52.35.Mw

The process of harmonic generation (HG) via intense laser pulses and the related production of short wavelength radiation in the extreme ultraviolet (xuv) range is well understood: odd high-order harmonics are produced on a plateau extending to a characteristic cutoff. Experimental efforts in this field are directed toward optimizing the photon yield at short wavelengths [1,2] even in the water window (2–4 nm) [3,4], and attaining ever shorter pulses in the attosecond regime [5,6]. Recently the issue of using HG for the production of phase-coherent short wavelength pulses has been put on the agenda [7,8] with the perspective of performing xuv and x-ray metrology studies.

In particular for the latter applications, as well as for general spectroscopic applications, phase evolution and frequency chirp effects in the spectral content of the harmonics are very important. Three decades ago Yablono-vitch already alluded to self-phase modulation effects by the incident laser beam causing a temporal change of the index of refraction $n(t)$ along a path z , therewith inducing a phase change $\phi(t) = -n(t)2\pi\nu_f z/c$ on the fundamental laser frequency ν_f [9]. The variation in phase results in an instantaneous frequency shift $2\pi\Delta\nu(t) = d\phi(t)/dt$ dubbed a chirp. In HG the phenomenon of multiphoton ionization (MPI) of the medium occurring in the laser focus imposes a change of the refractive index due to the free electron contribution, $n_e(t) \sim 1 - e^2 N_e(t)/(8\pi^2 m_e \epsilon_0 \nu^2)$, where e , m_e are the electron charge and mass, respectively, ϵ_0 is the vacuum dielectric constant, and $N_e(t)$ is the free electron density. During MPI n_e decreases, resulting in a blueshift of the harmonics, as was observed by Macklin *et al.* [10] and by Wahlström *et al.* [11]: the frequency of the q th-order harmonic ν_q was found to deviate from $q\nu_f$ by several percentage points. Extreme effects of optical field ionization-induced spectral shifts (all towards the blue) were observed by Bolton *et al.* [12]. Besides these collective effects, including the phenomenon of an intensity dependent index $n(I)$, the Kerr effect, also effects of blueshifts associated with single-atom response in HG were observed [13], however, only occurring for very short pulses (< 30 fs).

The present work seeks to explain experimentally observed features on harmonic frequency shift using laser pulses of $\tau = 300$ ps duration in the saturated intensity regime by including plasma dynamics effects and HG from ions. The experimental setup [14] and the procedures to obtain detailed information on the average chirp-induced shift in the harmonic spectrum [15] have been previously published. Here we present more detailed and refined measurements of average chirp-induced shifts on the 9th harmonic (H9) generated in a xenon gas jet. The central observation [as displayed in Fig. 1(b)] entails that the shifts, as a function of laser intensity I_0 in the focus ($f = 15$ cm), exhibit either a trend toward the *blue* or to the *red*, depending on particle density N in the focal region, which

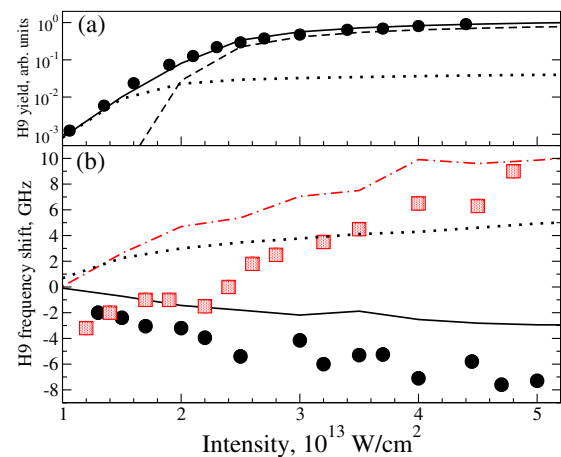


FIG. 1 (color online). (a) H9 intensity on a relative scale at density $N_1 = 1.2 \times 10^{17}$ cm⁻³; circles show experimental data and the full line is calculation based on the plasma dynamical model (see text). Contribution of atoms and ions is given by the dotted and dashed lines, respectively. (b) H9 frequency shift; black circles and shadowed squares show measured data at N_1 and N_2 (4.2×10^{17} cm⁻³), respectively; full line and dot-dashed line are calculation with contribution of atoms and ions including plasma dynamics for densities N_1 and N_2 , respectively; dotted line is calculation with contribution of atoms alone for density N_1 .

is set by changing the valve backing pressure. The interaction length is $L \sim 1$ mm. Measurements were performed at two gas densities: $N_1 = 1.2 \times 10^{17} \text{ cm}^{-3}$ and $N_2 = 4.2 \times 10^{17} \text{ cm}^{-3}$.

These measurements exploit the unique aspects of continuous tunability of the HG setup, as well as the narrow bandwidth, allowing for highly accurate frequency calibration in the xuv at 0.5 GHz [15]. As was described previously [14] the operation of the laser system involves a stage of amplification of a continuous wave (cw) beam in a sequence of three pulsed-dye amplifiers and further amplification in Ti:sapphire. Continuous tuning of the harmonic frequency is performed by scanning the cw laser frequency, ν_{cw} . Accurate frequency measurement in the xuv is accomplished by recording the absorption of H9 in an Ar gas jet while scanning the cw laser frequency at $\lambda_{\text{cw}} \sim 780$, such that the harmonic frequency spans across the transition $3p^6 1S_0 \rightarrow 3p^5 3d[3/2]_1$ at a frequency of $\nu_{\text{Ar}} = 3458611.8 \pm 0.3$ GHz [16,17]. The cw laser frequency ν_{cw} is simultaneously recorded during the measurements. The net harmonic frequency shift is then determined as the difference between ν_{Ar} and the peak of the absorption line, obtained from a least-square-fit on the experimental data points on a scale of $9\nu_{\text{cw}}$. Apart from the trend toward the *blue* with increasing focal intensities at high gas densities (N_2) and the trend toward the *red* for low gas densities (N_1), an offset frequency shift at low focal intensities is revealed in Fig. 1(b). This phenomenon is attributed to the properties of the fundamental laser radiation and will be addressed first before proceeding to an explanation of the harmonic chirp features.

In pulsed-dye amplifiers frequency chirp effects due to time-dependent gain are known to play a role [18]. In a separate setup the cw carrier beam was overlapped with the pulsed output of the dye amplifiers and transmitted through an etalon to register the net frequency shift induced by the chirp in the amplification. Results as a function of wavelength in the range 750–790 nm, shown in Fig. 2(a), display the typical behavior of sign-reversal when tuning over the peak of the dye gain curve [18]. At $\lambda_{\text{cw}} \sim 780$ nm the dye amplifier induces a redshift on the fundamental. It is verified in similar test experiments that the subsequent amplification of the output from the dye amplifiers in Ti:sapphire amplifiers and further optical components

used do not induce any significant extra chirp in the amplified pulse. The setting of the laser intensity I_0 in the range $1\text{--}5 \times 10^{13} \text{ W/cm}^2$ is achieved using a combination of a half-wave plate and a thin-film polarizer; hence the chirp on the fundamental pulse is intensity independent. The measurements of the chirp on the fundamental ν_f , as well as the harmonic frequency shift (Fig. 1) are all referenced against the cw carrier frequency of the laser system.

A second set of test experiments entail H9 production in *krypton* at an intensity of $1.4 \times 10^{13} \text{ W/cm}^2$. This is below the saturation intensity in krypton, determined at $I_s(\text{Kr}) \sim 2.5 \times 10^{13} \text{ W/cm}^2$ by recording the photo-electron yield in the focus vs intensity. For xenon a value of $I_s(\text{Xe}) \sim 10^{13} \text{ W/cm}^2$ is found. Both these values are in good agreement with a closed-form solution of MPI rate equations [19]. Results of H9 frequency shift as a function of krypton gas density in the focal region are shown in Fig. 2(b), displaying a constant redshift of 2.1 GHz. These measurements are performed using as frequency ruler in the xuv the same Ar transition used for the measurement with xenon, i.e., $\lambda_{\text{cw}} \sim 780$. The combination of the results of Fig. 2 is interpreted as follows: in the below-saturation regime the fundamental laser pulse induces an offset H9 frequency shift that is not related to the process of HG itself. This we regard as an explanation for the offset frequency shifts observed for H9 in *xenon* at low intensity, as occurring in Fig. 1(b). It is noted that this net H9 redshift offset cannot be derived from a simple multiplication by a factor of 9 of the measured net frequency shift of the fundamental pulse, since it is the result of a dynamic average of the chirp of the fundamental pulse involving the harmonic generation efficiency during the pulse time duration.

The striking feature of a redshifted harmonic might in principle be related to various physical phenomena. Since the atoms will ionize completely already before the peak of the pulse for $I_0 > I_s$, the Kerr effect of the neutrals might cause a redshift. However, based on a measured Kerr factor $n_2(\text{Xe}) \sim 10^{-20} \text{ cm}^2/\text{W}$ for a gas density of $N_0 = 3 \times 10^{17} \text{ cm}^{-3}$ [20], the maximum redshift of H9 is on the order of $(9n_2 I_0 L)/(\lambda \tau) \sim 10$ MHz, and hence negligible. Recently, significant spectral redshifts were reported as a result of cluster formation in the gas jet [21]. However, no significant clustering is expected at the opening orifice of the pulsed valve, where H9 is produced. Moreover, the

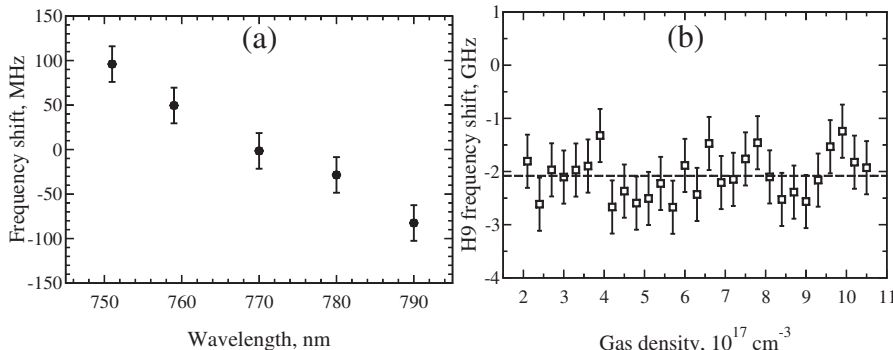


FIG. 2. Data providing information on the frequency chirp on the fundamental ν_f . (a) Net average frequency shift as a result of a chirp in the dye amplifiers as a function of wavelength over the gain curve of the dye used in the pulsed-dye amplifier, LDS 765. (b) Chirp-induced shift on H9 when using krypton as nonlinear medium at $I_0 = 1.4 \times 10^{13} \text{ W/cm}^2$, in the regime below saturation, again at $\lambda_{\text{cw}} = 780$ nm using the $3d'$ Ar resonance as frequency ruler.

redshift from clusters should increase with gas density, the opposite of what is actually observed (additional measurements for H9 in Xe performed in the range 10^{17} – 10^{18} cm^{-3} show a gradually increasing blueshift trend). Electron-ion recombination also would reduce the electron density, therewith causing a redshift. Based on the observed density dependence recombination can be excluded as the major cause for the redshift (see also Ref. [15]), but it is taken into account in the plasma dynamical model (see below).

Electron losses from the interaction region arise also from free electron expansion during MPI. The derivative of the electron density, in the case of total ionization ($N_e \sim N$), is $|dN_e/dt|_{\text{exp}} \sim N/\tau_{\text{exp}}$, where the characteristic expansion time for free electrons is $\tau_{\text{exp}} \sim 2R/V_{\text{th}}$, with $V_{\text{th}} \sim 6 \times 10^7 T_e^{1/2}$ the electron thermal velocity in cm/s, T_e in eV, and R , the laser spot radius, in cm. However, free expansion is realistic as long as the Debye length λ_D , i.e., the spatial range at which electrons are trapped by the ion field, is larger than the laser spot size, $\lambda_D \sim 8 \times 10^2 (T_e/N_e)^{1/2} > 2R$. This imposes a limit on the electron derivative $|dN_e/dt|_{\text{exp}} < 4 \times 10^{13} T_e^{3/2} / (2R)^3$. In our case, $T_e \sim 1$ eV and $2R \sim 3 \times 10^{-3}$ cm, thus $|dN_e/dt|_{\text{exp}} < 10^{21}$ cm^{-3}/s . Hence the maximum frequency shift one can expect from free electron expansion is 3 kHz, much smaller than the observed shift.

The strong density gradient that allows some electrons to escape from the small interaction volume determines a positive charge imbalance followed by an ion expansion. The time evolution of the radial ion profile evolves like a shock wave [22] that draws away the *trapped electrons* from the interaction region. The time constant of ion expansion is related to the ion plasma frequency, i.e., $\tau_i = 2\pi\sqrt{(\epsilon_0 m_i)/(e^2 N_i)}$, where N_i and m_i are the density and mass of ion, respectively. To estimate the frequency shift during the ion expansion we assume $|dN_e/dt|_i \sim N_e/\tau_i$ from which a frequency shift for H9 given by $(-9e^2 L N_e)/(8\pi^2 \epsilon_0 m_e c \nu \tau_i) \sim -2$ GHz is expected at $N_e \sim N_i = 10^{17}$ cm^{-3} . This result is qualitatively consistent with the experimental findings.

From the previous discussion, we infer that a quantitative explanation of the experimental results requires a detailed approach to the dynamics of charges combined with HG both by atoms and ions. The plasma dynamics is modeled by a two-fluid approach in a cylindrical geometry (ρ, z) . The basic set of equations contains motion and continuity equations for electrons and ions coupled by the electric field due to the different mobility of charges [23]. The continuity equations include the rates of the MPI process, recombination, and secondary impact ionization. In addition, two equations account for the electron heating due to inverse bremsstrahlung absorption and for the ion-electron thermal exchange, although the latter has a negligible effect during the laser pulse. The two-fluid model has been selected, instead of a simpler hydrodynamic model, because we expect a relatively large charge

imbalance due to the combined effects of the electron heating and the steep density gradient, which enhances the radial electron mobility. To simplify the model, we include in the equations of motion only the radial component of the electric field E_ρ , which can be directly integrated from the Maxwell equation, i.e., $E_\rho(\rho, t) = \frac{e}{\epsilon_0 \rho} \int_0^\rho (N_i(\rho, t) - N_e(\rho, t)) \rho d\rho$. In fact, the charge density is almost uniform along z since the laser confocal parameter is larger than the interaction length. Moreover, the interaction length is much larger than the radial spot size and hence the expansion along z reduces approximately linearly.

For the mechanism of HG we assume a classical picture based on the one-dimensional soft core potential

$$V_j(X_e(\rho, t)) = \frac{Z_j e}{4\pi\epsilon_0 \sqrt{a_j^2 + X_e^2(\rho, t)}}, \quad (1)$$

where the index $j = a, i$ refers to atoms and ions, respectively, Z_j and a_j are chosen to give the correct nuclear charge and ionization energy, and $X_e(\rho, t)$ is the position of the electron driven by the external laser field. The contribution to the H9 electric field entering the propagation equation is worked out classically from the Fourier analysis of the modulating term of the electron acceleration

$$\frac{Z_j e^3}{4\pi\epsilon_0^2 c^2 m_e} F^{-1} \left[F_9 \left[\frac{N_j(\rho, t) X_e(\rho, t)}{[a_j^2 + X_e^2(\rho, t)]^{3/2}} \right] \right], \quad (2)$$

where F_9 represent the Fourier transform at the frequency 9ν , F^{-1} the inverse Fourier transform, and $N_j(\rho, t)$ the atomic and ionic density as evaluated by the plasma dynamical model. The harmonic field at the exit of the medium $E_{9,j}(\rho, t)$ is evaluated after integration of the propagation equation along the z axis, hence including phase-matching.

The total harmonic yield is then given by $\int_0^T \times \int_0^R I_{9,j}(\rho, t) \rho d\rho dt$, where T is the time when harmonic generation stops. The harmonic intensity $I_{9,j}(\rho, t)$ is proportional to $|E_{9,j}(\rho, t)|^2$ for atoms or ions alone as emitter and to $|E_{9,a}(\rho, t) + E_{9,i}(\rho, t)|^2$ when both emitters are considered. In Fig. 1(a) the thus obtained H9 yield is plotted. The very good agreement between the experimental data and the calculation assuming both atoms and ions as emitters demonstrates the validity of the present theoretical approach to the HG process. The calculations show further that at intensities of 2×10^{13} W/cm² the ions take over as dominant HG emitters over the atoms. Calculations considering only neutrals as H9 emitters cannot explain the harmonic yield at the higher intensities. We observe that saturation of the harmonic intensity depends on depletion of the emitters, both for atoms and ions, even if the underlying mechanisms are different. In particular, for ionic HG the depletion is due to the ion expansion, whereas recombination is a negligible effect. For atoms, the onset of ionization reduces the effective time for HG although it

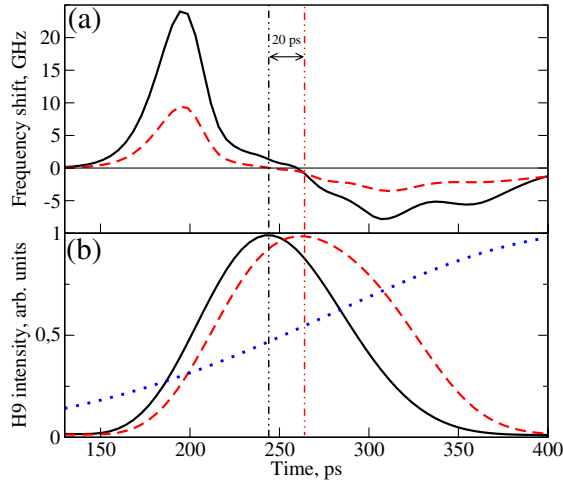


FIG. 3 (color online). Results of the calculations of the present plasma dynamical model for $I_0 = 4 \times 10^{13}$ W/cm². In both panels, the full (dashed) lines are for density N_2 (N_1). (a) Time evolution of the frequency chirp of the fundamental laser pulse averaged over the radial profile. (b) Time evolution of the harmonic intensity averaged over the radial profile. The dotted line represents the pulse envelope of the fundamental. The vertical dash-dotted lines serve to indicate the temporal peak of the harmonic intensity profile.

would be enhanced by the increase of laser intensity. Note that the radial integration is strictly required since the depletion along the laser axis is so strong as to give a decrease of harmonic generation for $I_0 > 2 \times 10^{13}$ W/cm².

In principle, the Fourier analysis of the overall response of medium yields the harmonic frequency shift. However, the very large temporal and spatial dependencies of the harmonic shift compels us to select a wide frequency window of integration leading to a tremendous increase of the computing time especially at higher gas densities. To speed up routine calculations and to facilitate the evaluation of different contributions to the shift, we compute the shift from a weighted average of the instantaneous H9 shift according to the following equation:

$$\Delta\nu_9 = \frac{\int_0^T \int_0^R I_9(\rho, t) 9\Delta\nu(\rho, t) \rho d\rho dt}{\int_0^T \int_0^R I_9(\rho, t) \rho d\rho dt}, \quad (3)$$

where $\Delta\nu(\rho, t) = -\nu(L/c)dn_e(\rho, t)/dt$. However, we have validated the correspondence of this method for various conditions. Results on the harmonic chirp shift are plotted in Fig. 1(b). The phenomenon of chirp-induced redshifted trends (as a function of laser intensity) at low gas densities (N_1), and a similar blueshifted trend at higher gas densities (N_2) is explained by the model including both atoms and ions as emitters. A calculation assuming only neutrals as H9 emitters produces blueshifts as expected from MPI. We note that the zero-offset of the experimental data is proven to be related to an intrinsic chirp in the fundamental laser pulses.

Figure 3 shows further details following from the model at the two gas densities N_2 and N_1 and for a laser intensity of 4×10^{13} W/cm², which are particularly significant configurations to elucidate the role of the plasma evolution. Figure 3(a) shows the frequency chirp of the fundamental averaged over the radial profile, while Fig. 3(b) reports the H9 yield from ions averaged over the radial profile with the envelope of the fundamental laser pulse as reference. The vertical dash-dotted lines indicate the temporal peak of the H9 intensity profile.

From inspection of Fig. 3 it is evident that at density N_1 the H9 intensity peak occurs when the fundamental beam undergoes a frequency redshift, leading to the observed net redshift in H9, while at N_2 the H9 intensity peak comes 20 ps earlier, during blueshift of the fundamental, thus resulting in a net H9 blueshift. This is the explanation for the central and striking observations of redshifts and blueshifts under varying density conditions.

This study is supported by the European Community, Integrated Infrastructure Initiative action (RII3-CT-2003-506350), and the Fondazione Cassa di Risparmio di Pisa, Grant No. 130/03. F.G. wishes to thank the Laser Centre Vrije Universiteit for hospitality.

*Email address: brandi@df.unipi.it

†Electronic address: www.nat.vu.nl/~laser/

- [1] A. Rundquist *et al.*, *Science* **280**, 1412 (1998).
- [2] R. A. Bartels *et al.*, *Science* **297**, 376 (2002).
- [3] C. Spielmann *et al.*, *Science* **278**, 661 (1997).
- [4] E. A. Gibson *et al.*, *Science* **302**, 95 (2003).
- [5] P. M. Paul *et al.*, *Science* **292**, 1689 (2001).
- [6] A. Baltuska *et al.*, *Nature (London)* **421**, 611 (2003).
- [7] S. Witte *et al.*, *Science* **307**, 400 (2005).
- [8] R. J. Jones *et al.*, *Phys. Rev. Lett.* **94**, 193201 (2005).
- [9] E. Yablonovitch, *Phys. Rev. Lett.* **31**, 877 (1973).
- [10] J. J. Macklin, J. D. Kmetec, and C. L. Gordon III, *Phys. Rev. Lett.* **70**, 766 (1993).
- [11] C.-G. Wahlström *et al.*, *Phys. Rev. A* **48**, 4709 (1993).
- [12] P. R. Bolton *et al.*, *J. Opt. Soc. Am. B* **13**, 336 (1996).
- [13] H. J. Shin *et al.*, *Phys. Rev. Lett.* **83**, 2544 (1999).
- [14] F. Brandi, D. Neshev, and W. Ubachs, *Phys. Rev. Lett.* **91**, 163901 (2003).
- [15] F. Giammanco *et al.*, *Laser Phys.* **15**, 328 (2005).
- [16] I. Velchev, W. Hogervorst, and W. Ubachs, *J. Phys. B* **32**, L511 (1999).
- [17] L. Minnhagen, *J. Opt. Soc. Am.* **63**, 1185 (1973).
- [18] N. Melikechi, S. Gangopadhyay, and E. E. Eyler, *J. Opt. Soc. Am. B* **11**, 2402 (1994).
- [19] B. Chang, P. R. Bolton, and D. N. Fittinghoff, *Phys. Rev. A* **47**, 4193 (1993).
- [20] E. T. J. Nibbering *et al.*, *J. Opt. Soc. Am. B* **14**, 650 (1997).
- [21] K. Y. Kim *et al.*, *Phys. Rev. A* **71**, 011201(R) (2005).
- [22] C. G. Durfee III, J. Lynch, and H. M. Milchberg, *Phys. Rev. E* **51**, 2368 (1995).
- [23] Y. P. R. Ya. B. Zel'dovich, *Physics of Shock Waves and High Temperature Hydrodynamic Phenomena* (Academic Press, New York, 1966).